Angewandte Chemie
Eine Zeitschrift der Gesellschaft Deutscher Chemiker

Supporting Information

A Minimal Functional Complex of Cytochrome P450 and FBD of Cytochrome P450 Reductase in Nanodiscs

*Elke Prade[+], Mukesh Mahajan[+], Sang-Choul Im, Meng Zhang, Katherine A. Gentry, G. M. Anantharamaiah, Lucy Waskell, and Ayyalusamy Ramamoorthy**

anie_201802210_sm_miscellaneous_information.pdf

Materials

Potassium phosphate (monobasic and dibasic) and benzphetamine were purchased from Sigma-Aldrich (St. Louis, MO). 1,2-dimyristoyl-sn-glycero-3-phosphocholine (DMPC) was purchased from Avanti Polar Lipids, Inc. (Alabaster, AL). Deuterium oxide (D_2O) and ^{15}N Celtone Base Powder were purchased from Cambridge Isotope Laboratories (Tewksbury, MA). The 5-mm symmetrical D_2O-matched Shigemi NMR microtubes were purchased from Shigemi, Inc (Allison Park, PA).

Methods

Expression and purification of proteins. FBD of rat CPR was purified as described previously [1]. The fl-FBD gene is encoded on a pSC plasmid, and is preceeded by the OmpA signal peptide [2]. Briefly, fl-FBD was expressed in *E. coli* C41 cells in either LB medium for unlabeled protein, or M9 medium for U-^{15}N or U-^{15}N/^{13}C labeled samples, supplemented with 5 nM FMN. Protein expression was induced at OD_{600} = 0.7 by adding 0.4 mM IPTG to the cultures for 16 h at 30 °C. After cell harvest at 6000 x g and 4 °C, the cells were lysed by 30 µg/ml lysozyme and protease inhibitor in Tris-Acetate buffer pH 7.4 for 30 mins at 4 °C, followed by sonication (with 1 s on and 1 s off pulses) for 5 mins. The membrane fraction was pelleted by ultracentrifugation at 105,000 x g and 4 °C for 45 mins, and further treated with 0.3% (v/v) Triton X-100 for 16 h at 4 °C. The solubilized membrane proteins were purified by DEAE anion exchange chromatography twice. For this purpose, the protein was loaded onto the column and eluted using a NaCl gradient ranging from 0.2 M to 0.5 M in Tris-Acetate pH 7.4 containing 1 µM FMN, 0.3% (v/v)

sodium cholate. Full-length CYP2B4 was expressed and purified as described in the literature [3].

Reconstitution of full-length proteins in nanodiscs. Empty nanodiscs were produced from the 4F peptide and DMPC in 40 mM sodium phosphate pH 7.4. The 4F peptide was predissolved to a stock concentration of 10 mg/ml. DMPC was predissolved to 20 mg/ml and vortexed and sonicated to achieve a homogeneous suspension. The 4F peptide and DMPC were mixed at a 1:1.5 (w/w) ratio, and incubated for 16 h at 37 °C with gentle agitation. The nanodiscs were purified by size exclusion chromatography (SEC) using a Superdex 200 Increase 300/10 GL column operated on an ÄKTA purifier (GE Healthcare, Freiburg, Germany), and incubated with fl-FBD or fl-CYP2B4 at molar ratios of 1:1.2 (protein/nanodisc), and incubated for 16 h at 25 °C with gentle agitation. The reconstitution was further purified by SEC. Fractions showing absorbance at 412 nm (CYP2B4) or 454 nm (FBD) were pooled and used for further analysis. In order to form a complex, fl-FBD was added to purified CYP2B4 reconstituted in nanodiscs at a molar ratio of 1:1. The empty nanodiscs, proteins, and reconstituted proteins were subjected to dynamic light scattering (DLS) measurements on a DynaPro NanoStar instrument (Wyatt Technology Corp., Santa Barbara, USA) at 25 °C for 10 acquisitions of 5 s each. DLS and SEC measurements confirm the increase of the hydrodynamic radius after stepwise incubation with fl-CYP2B4 and fl-FBD. The relative ratio of SEC purified reconstituted protein complex in nanodiscs was calculated using the absorbance at 417 nm and 454 nm for CYP2B4 and FBD, respectively (Figure S5).

SAXS measurements. SAXS data were acquired at the BioCAT beamline at Sector 18-ID of the APS in Argonne National Laboratory, Chicago. Both empty nanodiscs and redox complex fl-CYP2B4-FBD anchored in 4F-DMPC nanodiscs were prepared (as mentioned above) at 60 μM and ~20 μM, respectively, in 1 ml in buffer containing 40 mM potassium phosphate, pH 7.4. Both nanodiscs and reconstituted protein complex purified from size exclusion chromatography (SEC) were delivered using an autosampler with continuous unidirectional flow and recorded with 1 s exposure. Data was acquired as previously described elsewhere [4]. Scattering intensity plots (Figure 2c) are the average of triplicate experiments and subtracted with buffer. SAXS data was processed using the program PRIMUS in ATSAS package [5]. The scattering curves were first analyzed for aggregation using the Guinier region. The forward scattering I(0) and the radius of gyration, R_g, were computed using the Guinier approximation. R_g provides a measure of the overall size of the macromolecule (Figure S4a). The pair distance distribution function P(r), was computed from the extended scattering patterns using the indirect transform program GNOM in PRIMUS. The maximum dimension of the particle, D_{max}, estimated from the P(r) function satisfying the condition P(r)=0 (Figure S4c-d). The molecular folding and compactness of reconstituted full-length redox complex in nanodisc were analyzed by using the normalized Kratky plot (Figure S4f). Bell-shaped profile from scattering pattern in a normalized Kratky plot demonstrates the folded protein. *Ab initio* shape reconstruction of nanodiscs and redox complex (fl-CYP2B4-fl-FBD) anchored in nanodiscs was obtained by DAMMIN/DAMMIF module in PRIMUS from ATSAS package (Figures 2d and S4e).

NMR experiments. All NMR experiments were carried out at 298 K (25 °C). 3D HNCA, HNCACB and CBCA(CO)NH [6-10] experiments were performed on a Bruker 900 MHz NMR spectrometer equipped with a triple-resonance cryoprobe (^{1}H, ^{15}N, ^{13}C) on a sample containing 250 µM protein and 10% D_2O. All other NMR experiments were carried out on a Bruker Avance II 600 MHz equipped with a triple-resonance cryoprobe (^{1}H, ^{15}N, ^{13}C) at FBD concentrations of 100 µM. 2D ^{1}H-^{15}N TROSY HSQC [11, 12] spectra were recorded with 256 t_1 increments.

Sequential assignment and analysis of CPSs, signal intensities was performed using CcpNmr Analysis 2.4.1 [13]. Secondary structural elements were predicted using TALOS+ [14] and random coil values as reported by Wishart *et al* [15]. Chemical shift perturbations (CSP) were calculated from ^{1}H-^{15}N TROSY HSQCs using the following equation:

To record solvent PRE (sPRE) data, 1 mM of the lanthanide [Gd(DTPA-BMA)] [16] was added to the sample and measured immediately. Residues of fl-FBD in the binding interface to fl-CYP2B4 will be protected from the sPRE singal quenching upon complex formation. This extend (ΔQuenching) was determined by the following equation:

$$\Delta\text{Quenching} = (\text{complex}_{\text{sPRE}}/\text{complex}_{\text{ref}})-(\text{fl-FBD}_{\text{sPRE}}/\text{fl-FBD}_{\text{ref}})$$

Structural model calculation. A structural model for the globular domain of FBD was calculated using the Chemical-Shift-ROSETTA (CS-ROSETTA) server from the Biological Magnetic Resonance Data Bank.[17-20] CS-ROSETTA is a robust tool for *de novo* protein structure generation, using ^{13}C,

^{15}N and ^{1}H NMR chemical shifts as input. It employs SPARTA-based selection of protein fragments from the PDB, in conjunction with a regular ROSETTA Monte Carlo assembly and relaxation procedure, to generate structures of minimized energies.

CYPP450-FBD complex structure calculation. HADDOCK 2.2 webserver [21] was used to dock FBD and CYP450 based on a number of ambiguous restraints derived from NMR and site-directed mutagenesis experiments [22] (*Table 1*). It involves rigid-body docking, followed by molecular dynamics simulations that allow selected amino acid side chains, as well as parts of the backbone, to move freely to improve the complementarity and electrostatic interactions at the interface. For this calculation, we used the X-ray structure of rat FBD (PDB structure: 1AMO [23]; Val64 to Ala-235 and the heme domain of CYP2B4 (PDB code 1SUO [24]). Docking was performed using default parameters in the absence of a membrane environment. However, it must be noted that all NMR, SAXS and catalytic data were acquired on membrane anchored full-length proteins. Ligand topology and parameter files were generated from the PRODRG2 server [25]. NMR based CSPs and differential line broadening data were used as proximity restraints to guide the docking process whereby rigid body docking follows the semi-flexible refinement and energy minimization in explicit solvent to allow the free movement of backbone and side chain atoms of the selected amino acids to improve the intermolecular packing at protein interface. The active ambiguous restraints were chosen based on literature for CYP2B4 [22] and experimentally determined NMR restraints for FBD. Rigid body energy minimization was

used for docking 1000 structures of the complex. The second step included semi-rigid simulated annealing from which the best 200 structures were selected for refinement. The best 200 structures were further refined with explicit solvent in an 8.0 Å shell of TIP3P water molecules. Models are displayed using PyMOL [26].

Stopped-flow measurement of electron transfer from hydroquinone FMN to oxyferrous fl-CYP2B4 reconstituted in 4F-peptide based lipid nanodiscs. All experiments were performed at 15 °C under anaerobic conditions using a Hi-Tech stopped-flow apparatus in a glove box ($[O_2]$<<2ppm). All stock solutions (proteins and benzphetamine) were prepared in degassed and air saturated 40 mM potassium phosphate buffer pH 7.4. Degassed and air saturated buffers were prepared by purging nitrogen and air, respectively for 30 minutes. Stock solutions of benzphetamine and protein were prepared at 1 mM and 3.5 mM, respectively in 40 mM potassium phosphate buffer pH 7.4. An equimolar amount of full-length proteins (CYP2B4 and FBD) in the nanodiscs was incubated overnight at 4°C in the glove box. After the addition of benzphetamine to the protein complex, the protein was stoichiometrically reduced with dithionite. The stoichiometric reduction of the protein complex yielded ferrous CYP450, and the 2-electron reduced FBD ($FMNH_2$) The 3-electron-reduced protein complex was loaded into the stopped-flow spectrophotometer and mixed with air-saturated potassium phosphate buffer buffer. Intermolecular electron transfer from FBD and to oxyferrous CYP450 was observed as oxidation of FBD at 585 nm.

Evolutionary conservation analysis. The ConSurf web server (http://consurf.tau.ac.il/2016/)[27-31] uses a query sequence or structure and analyzes the evolutionary pattern of the amino acids to reveal the regions important for structure and/or function.

Supplementary Figures:

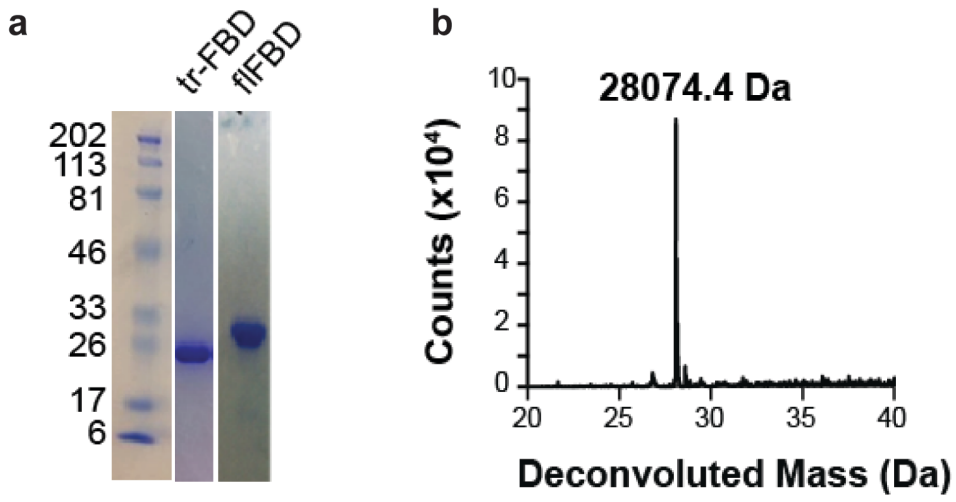

Figure S1: (a) SDS-PAGE of tr-FBD (21 kDa) and fl-FBD (28 kDa). (b) ESI mass spectrometry data for ^{15}N fl-FBD.

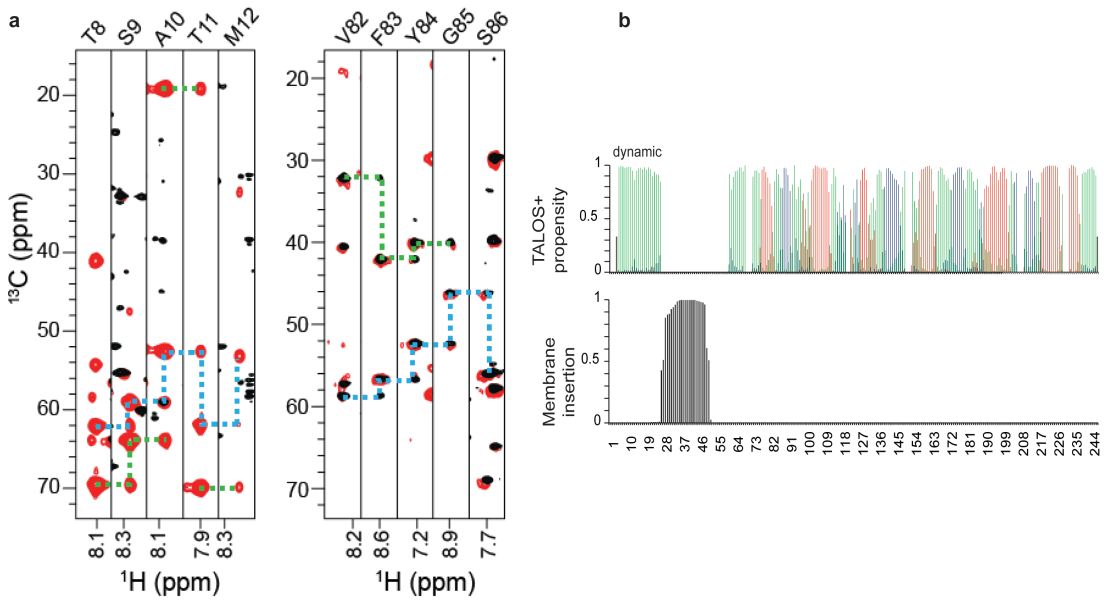

Figure S2: (a) Representative strips selected from 3D HNCACB spectra of tr-FBD in solution (black) and fl-FBD in nanodiscs (red). Peaks originating from C_α and C_β resonances are indicated in blue and green, respectively. (b) Upper panel: Secondary structural elements as predicted by TALOS+ [14]. Lower panel: Prediction of the transmembrane sequence based on TMHMM, a membrane protein topology prediction server [32]. The indicated secondary structural elements are highly comparable to those reported in the crystal structure of tr-FBD (PDB ID 4YAF) [33].

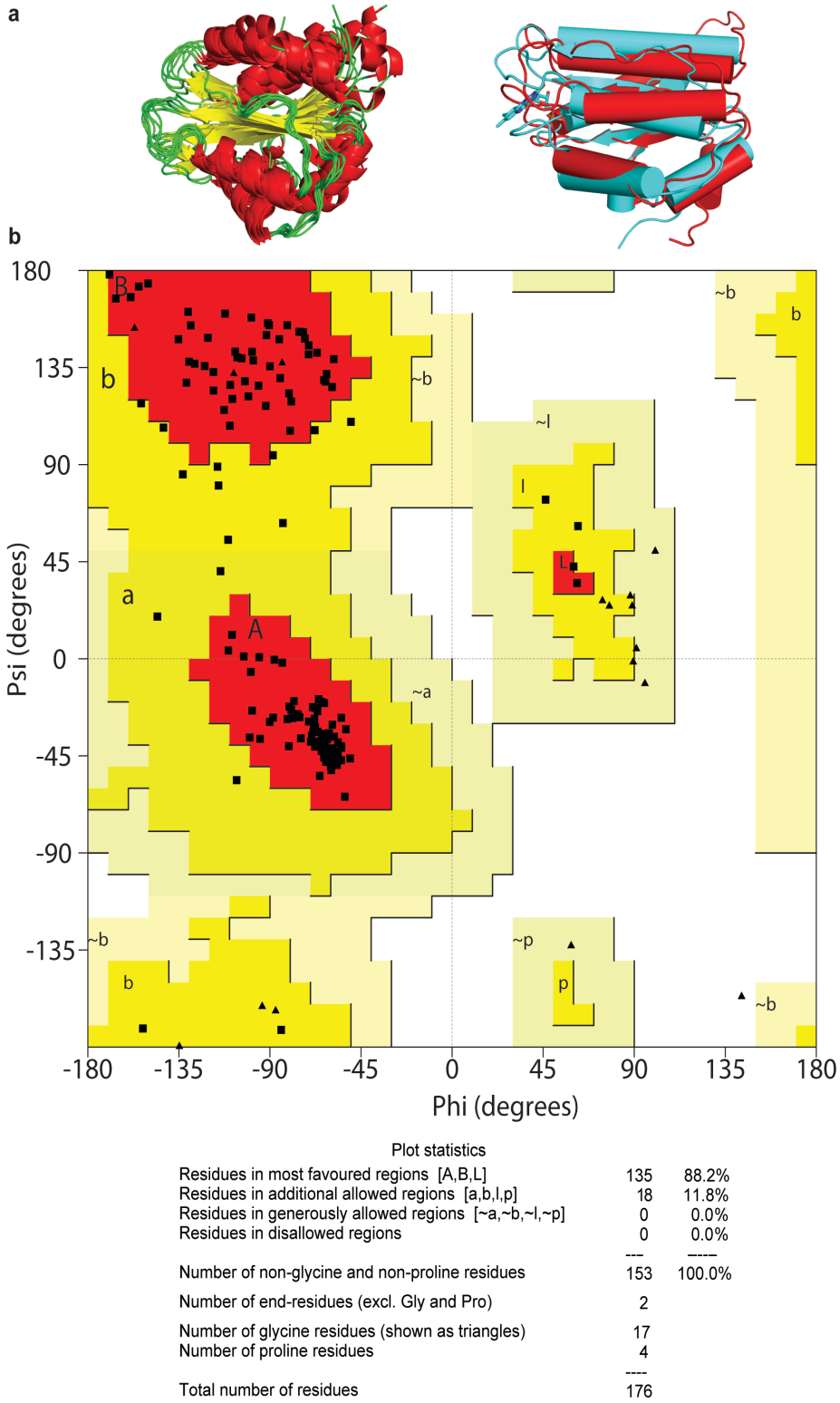

Plot statistics

Residues in most favoured regions [A,B,L]	135	88.2%
Residues in additional allowed regions [a,b,l,p]	18	11.8%
Residues in generously allowed regions [~a,~b,~l,~p]	0	0.0%
Residues in disallowed regions	0	0.0%
Number of non-glycine and non-proline residues	153	100.0%
Number of end-residues (excl. Gly and Pro)	2	
Number of glycine residues (shown as triangles)	17	
Number of proline residues	4	
Total number of residues	176	

Figure S3: (a) An ensemble of 10 lowest energy structural models determined using CS-ROSETTA showing the well-conserved *Rossman fold*. Right, Superimposed X-ray (cyan) and NMR (red) structures with r.m.s.d. values of ~3.0 Å. (b) Ramachandran plot generated by PROCHECK [34, 35] validation software showing the stereochemical quality of CS-ROSETTA [19] derived structural model of the soluble domain of fl-FBD anchored in nanodiscs.

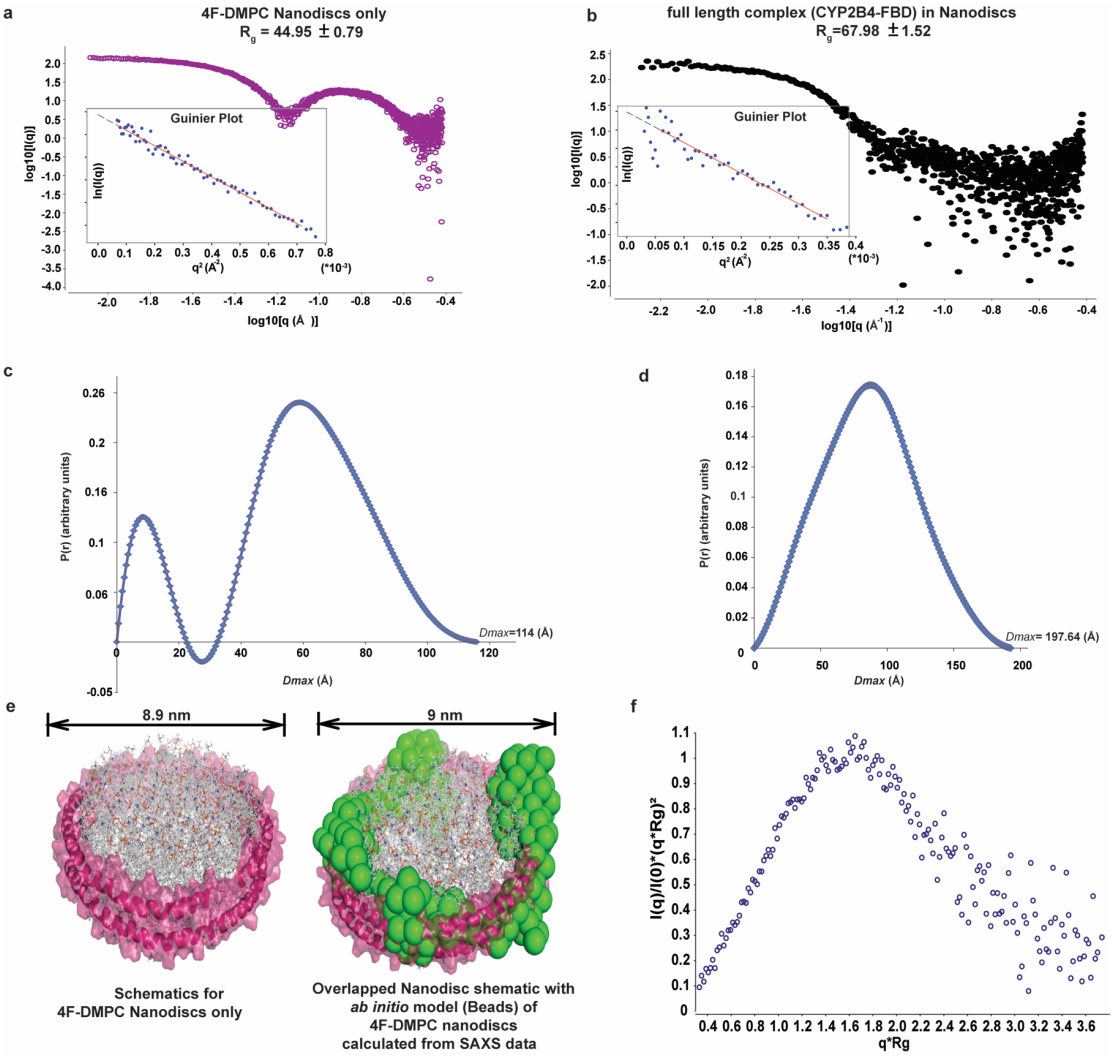

Figure S4: SAXS measurements and analysis of the fl-FBD fl-CYP2B4 complex in peptide-based nanodiscs. (a-b) SAXS curves in reciprocal (Fourier) space with linear Guinier region (inserts) demonstrate sample uniformity. Radii of gyration (R_g) calculated from Guinier plot of nanodiscs and reconstituted full-length redox complex (fl-FBD-fl-CYP2B4) are 44.95±0.79 and 67.98±1.52 Å, respectively. (c-d) Pair-distance distribution function (PDDF) of empty nanodiscs and the reconstituted redox complex obtained using indirect Fourier transform in GNOM module from ATSAS package. The region of negative contrast in empty nanodiscs is a characteristic property of hydrophobic acyl chains in lipid bilayers. This effect is present in both cases, however it is more pronounced in empty nanodiscs, as the relative concentration of acyl chains is higher. (e) Schematic representation of peptide-based nanodiscs (left) and overlapped *ab initio* model of peptide-based nanodisc (green) generated from SAXS data using the DAMMIN/DAMMIF module in Primus (right). (f) Normalized Kratky plot reveals a bell-shaped profile for the fl-FBD-fl-CYP2B4 complex reconstituted in nanodiscs. This experimental result further confirms the reconstitution of a properly folded protein-protein complex in peptide-based lipid nanodiscs. All SAXS data were analyzed using various modules of the ATSAS package [5].

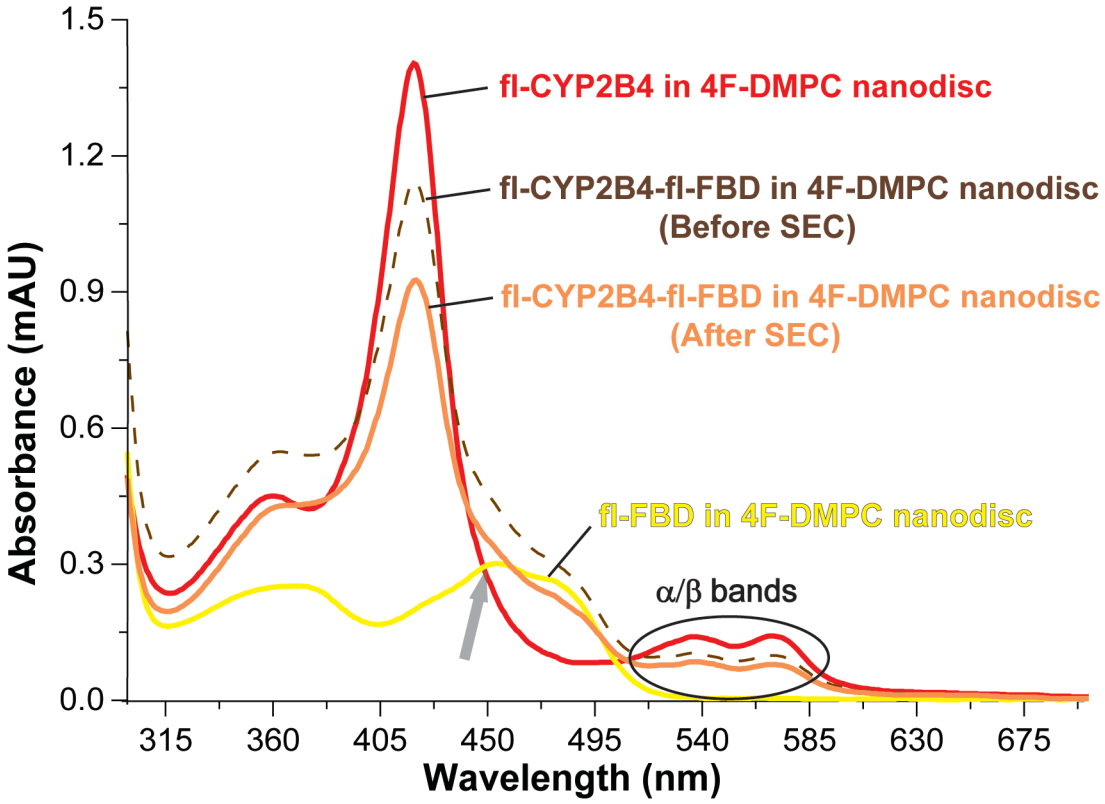

Figure S5: UV-Vis spectra for SEC purified nanodisc embedded CYP2B4 (red), FBD (yellow) and CYP2B4-FBD complex (orange). The absorption maxima at 417 nm and α/β bands at 530-585 nm are signature features of CYP2B4. However, FBD shows a broad band from 405-520 nm with absorption maxima at 454 nm. The presence of both full-length proteins (CYP2B4-FBD) in the nanodisc can be confirmed by the broad peak at ~ 450 nm (marked by an arrow) along with a peak at 417 nm and α/β bands at 530-585 nm. Based on the absorbance of the respective proteins in the complex (CYP2B4-FBD), the relative ratio of CYP2B4 to FBD was observed to be 0.95, indicative of 1:1 protein:protein ratio in the complex.

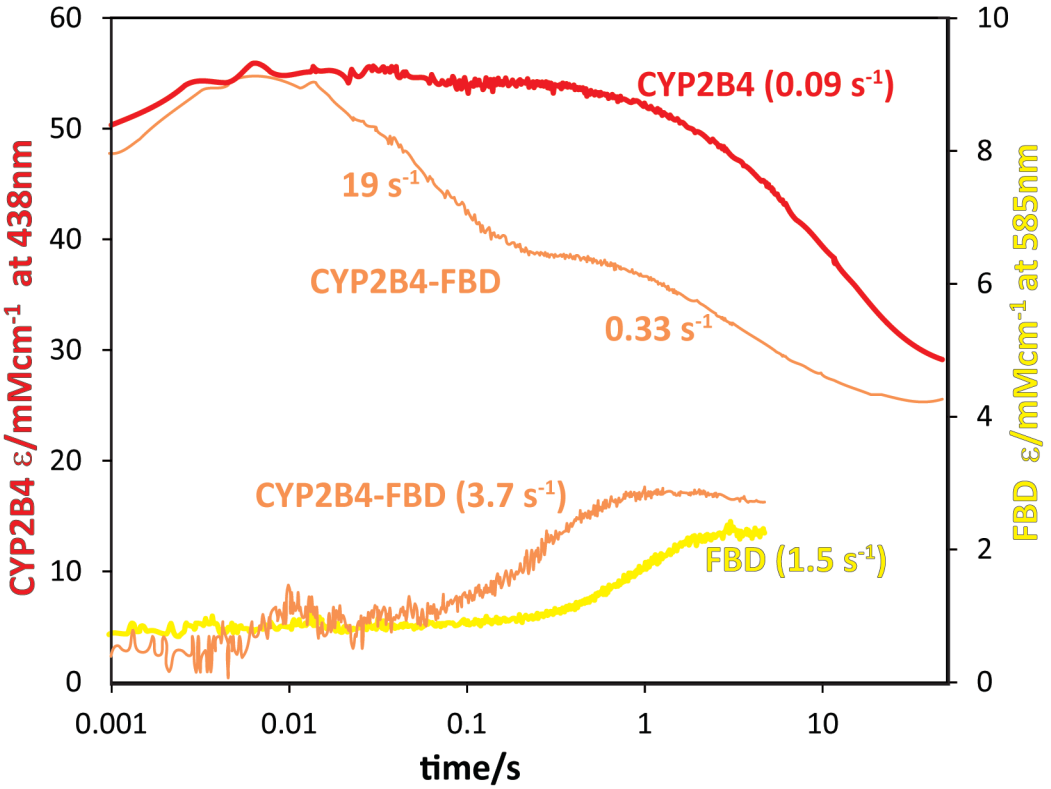

Figure S6: Stopped-flow data for electron transfer from fl-FBD to fl-CYP2B4. The proteins were incubated individually (yellow and red for FBD and CYP2B4, respectively), in complex (orange) with nanodiscs and the absorption changes were monitored.

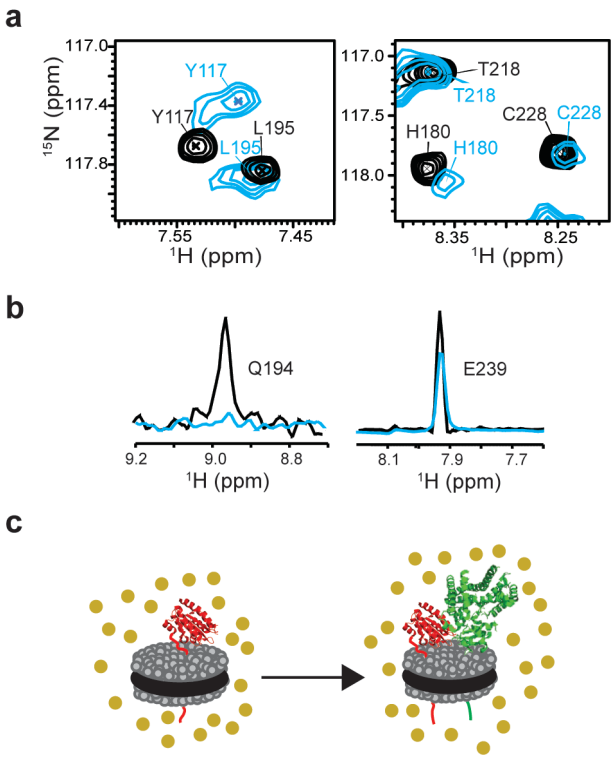

Figure S7: (a) Representative excerpts displaying CSPs experienced by Y117 and H180 of fl-FBD in nanodiscs without (black) and with fl-CYP2B4 (blue). (b) Representative ^{1}H-1D slices extracted from ^{1}H-^{15}N-TROSY-HSQC demonstrate attenuation of Q194 and preservation of E239 resonances from fl-FBD in nanodiscs without (black) and with fl-CYP2B4 (blue). (c) Schematic illustration of sPRE experimental setup; Gd (DTPA-BMA) (yellow) was added to fl-FBD or the fl-FBD-fl-CYP2B4 complex in nanodiscs.

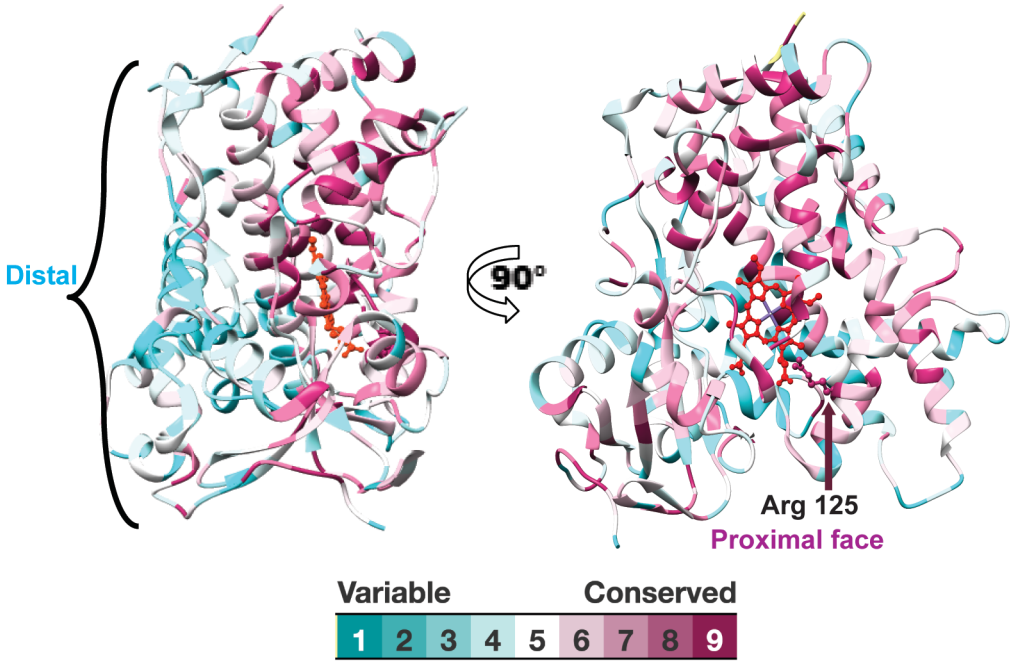

Figure S8: ConSurf analysis [30, 31] of fl-CYP2B4 based on the structural and functional importance of residues reveals conserved (purple-9) and variable residues (blue-1) present on proximal and distal sides of CYP450, respectively. R125 (ball and stick), located in the C-helix on the proximal side of fl-CYP2B4 is one of the most conserved residues and found to be important for electron transfer to heme.

Table 1: List of restraints used in HADDOCK simulations [21] for the full-length complex in nanodiscs. Active restraints on FBD site were obtained from TROSY based ^{15}N-HSQC experiments on full-length complex reconstituted in lipid nanodiscs, whereas site directed mutagenesis data [22] was used for CYP2B4.

	fl-FBD	**fl-CYP2B4**
Ambiguous active restraints	88, 116, 143, 146, 175, 177, 179	122, 126, 133, 135, 137, 422, 433

Table 2: Energy statistics of the lowest energy cluster of the FBD-CYP2B4 complex obtained using HADDOCK server [21].

HADDOCK score	-106.0 +/- 6.0
RMSD from the overall lowest-energy structure	0.8 +/- 0.5
Van der Waals energy	-47.5 +/- 6.7
Electrostatic energy	-489.6 +/- 22.5
Desolvation energy	38.2 +/- 6.2
Restraints violation energy	10.7 +/- 16.27
Buried Surface Area	1991.0 +/- 125.0
Z-Score	-2.7

References

[1] R. Huang, M. Zhang, F. Rwere, L. Waskell, A. Ramamoorthy, *J Biol Chem* **2015**, *290*, 4843-4855.

[2] A. L. Shen, T. D. Porter, T. E. Wilson, C. B. Kasper, *J Biol Chem* **1989**, *264*, 7584-7589.

[3] A. S. Saribas, L. Gruenke, L. Waskell, *Protein Expr Purif* **2001**, *21*, 303-309.

[4] A. W. Malaby, S. Chakravarthy, T. C. Irving, S. V. Kathuria, O. Bilsel, D. G. Lambright, *J Appl Crystallogr* **2015**, *48*, 1102-1113.

[5] D. Franke, M. V. Petoukhov, P. V. Konarev, A. Panjkovich, A. Tuukkanen, H. D. T. Mertens, A. G. Kikhney, N. R. Hajizadeh, J. M. Franklin, C. M. Jeffries, D. I. Svergun, *J Appl Crystallogr* **2017**, *50*, 1212-1225.

[6] S. Grzesiek, A. Bax, *J Magn Reson* **1992**, *96*, 432-440.

[7] S. Grzesiek, A. Bax, *J Am Chem Soc* **1992**, *114*, 6291-6293.

[8] S. Grzesiek, A. Bax, *J Magn Reson* **1992**, *99*, 201-207.

[9] M. Sattler, *Prog Nucl Magn Reson Spectrosc* **1999**, *34*, 93-158.

[10] L. E. Kay, M. Ikura, R. Tschudin, A. Bax, *J Magn Reson* **1990**, *89*, 496-514.

[11] K. Pervushin, R. Riek, G. Wider, K. Wuthrich, *Proc Natl Acad Sci U S A* **1997**, *94*, 12366-12371.

[12] C. Fernandez, G. Wider, *Curr Opin Struct Biol* **2003**, *13*, 570-580.

[13] W. F. Vranken, W. Boucher, T. J. Stevens, R. H. Fogh, A. Pajon, M. Llinas, E. L. Ulrich, J. L. Markley, J. Ionides, E. D. Laue, *Proteins* **2005**, *59*, 687-696.

[14] Y. Shen, F. Delaglio, G. Cornilescu, A. Bax, *J Biomol NMR* **2009**, *44*, 213-223.

[15] D. S. Wishart, C. G. Bigam, J. Yao, F. Abildgaard, H. J. Dyson, E. Oldfield, J. L. Markley, B. D. Sykes, *J Biomol NMR* **1995**, *6*, 135-140.

[16] H. G. Hocking, K. Zangger, T. Madl, *Chemphyschem* **2013**, *14*, 3082-3094.

[17] O. F. Lange, P. Rossi, N. G. Sgourakis, Y. F. Song, H. W. Lee, J. M. Aramini, A. Ertekin, R. Xiao, T. B. Acton, G. T. Montelione, D. Baker, *Proceedings of the National Academy of Sciences of the United States of America* **2012**, *109*, 10873-10878.

[18] Y. Shen, P. N. Bryan, Y. He, J. Orban, D. Baker, A. Bax, *Protein Sci* **2010**, *19*, 349-356.

[19] Y. Shen, R. Vernon, D. Baker, A. Bax, *J Biomol NMR* **2009**, *43*, 63-78.

[20] Y. Shen, O. Lange, F. Delaglio, P. Rossi, J. M. Aramini, G. Liu, A. Eletsky, Y. Wu, K. K. Singarapu, A. Lemak, A. Ignatchenko, C. H. Arrowsmith, T. Szyperski, G. T. Montelione, D. Baker, A. Bax, *Proc Natl Acad Sci U S A* **2008**, *105*, 4685-4690.

[21] G. C. van Zundert, J. P. Rodrigues, M. Trellet, C. Schmitz, P. L. Kastritis, E. Karaca, A. S. Melquiond, M. van Dijk, S. J. de Vries, A. M. Bonvin, *J Mol Biol* **2016**, *428*, 720-725.

[22] A. Bridges, L. Gruenke, Y. T. Chang, I. A. Vakser, G. Loew, L. Waskell, *J Biol Chem* **1998**, *273*, 17036-17049.

[23] M. Wang, D. L. Roberts, R. Paschke, T. M. Shea, B. S. Masters, J. J. Kim, *Proc Natl Acad Sci U S A* **1997**, *94*, 8411-8416.

[24] E. E. Scott, M. A. White, Y. A. He, E. F. Johnson, C. D. Stout, J. R. Halpert, *J Biol Chem* **2004**, *279*, 27294-27301.
[25] A. W. Schuttelkopf, D. M. van Aalten, *Acta Crystallogr D Biol Crystallogr* **2004**, *60*, 1355-1363.
[26] Schrodinger, LLC, *The PyMOL Molecular Graphics System, Version 1.3r1*, **2010**.
[27] H. Ashkenazy, S. Abadi, E. Martz, O. Chay, I. Mayrose, T. Pupko, N. Ben-Tal, *Nucleic Acids Res* **2016**, *44*, W344-350.
[28] H. Ashkenazy, E. Erez, E. Martz, T. Pupko, N. Ben-Tal, *Nucleic Acids Res* **2010**, *38*, W529-533.
[29] G. Celniker, G. Nimrod, H. Ashkenazy, F. Glaser, E. Martz, I. Mayrose, T. Pupko, N. Ben-Tal, *Israel Journal of Chemistry* **2013**, *53*, 199-206.
[30] M. Landau, I. Mayrose, Y. Rosenberg, F. Glaser, E. Martz, T. Pupko, N. Ben-Tal, *Nucleic Acids Res* **2005**, *33*, W299-302.
[31] F. Glaser, T. Pupko, I. Paz, R. E. Bell, D. Bechor-Shental, E. Martz, N. Ben-Tal, *Bioinformatics* **2003**, *19*, 163-164.
[32] A. Krogh, B. Larsson, G. von Heijne, E. L. Sonnhammer, *J Mol Biol* **2001**, *305*, 567-580.
[33] F. Rwere, C. Xia, S. Im, M. M. Haque, D. J. Stuehr, L. Waskell, J. J. Kim, *J Biol Chem* **2016**, *291*, 14639-14661.
[34] R. A. Laskowski, M. W. MacArthur, D. S. Moss, J. M. Thornton, *J Appl Crystallogr* **1993**, *26*, 283-291.
[35] R. A. Laskowski, J. A. Rullmannn, M. W. MacArthur, R. Kaptein, J. M. Thornton, *J Biomol NMR* **1996**, *8*, 477-486.